

# Detection of [O III] at $z \sim 3$ : A Galaxy Above the Main Sequence, Rapidly Assembling Its Stellar Mass

Amit Vishwas ®, Carl Ferkinhoff ®, Thomas Nikola Stephen C. Parshley Justin P. Schoenwald Gordon J. Stacey Sarah J. U. Higdon ®, James L. Higdon ®, Axel Weiss ®, Rolf Güsten and Karl M. Menten Department of Astronomy, Cornell University, Ithaca, NY 14853, USA; vishwas © cornell.edu

Department of Physics, Winona State University, Winona, MN 55987, USA

Cornell Center for Astrophysics & Planetary Science, Ithaca, NY 14853, USA

Department of Physics and Astronomy, Georgia Southern University, Statesboro, GA 30460, USA

Max-Planck-Institut für Radioastronomie, Auf dem Hügel 69, D-53121 Bonn, Germany

Received 2017 November 28; revised 2018 February 23; accepted 2018 February 26; published 2018 April 5

#### **Abstract**

We detect bright emission in the far-infrared (far-IR) fine structure [O III] 88  $\mu$ m line from a strong lensing candidate galaxy, H-ATLAS J113526.3-014605, hereafter G12v2.43, at z=3.127, using the second-generation Redshift (z) and Early Universe Spectrometer (ZEUS-2) at the Atacama Pathfinder Experiment Telescope (APEX). This is only the fifth detection of this far-IR line from a submillimeter galaxy at the epoch of galaxy assembly. The observed [O III] luminosity of  $7.1 \times 10^9 \left(\frac{10}{\mu}\right) L_{\odot}$  likely arises from H II regions around massive stars, and the amount of Lyman continuum photons required to support the ionization indicate the presence of  $(1.2-5.2) \times 10^6 \left(\frac{10}{\mu}\right)$  equivalent O5.5 or higher stars, where  $\mu$  would be the lensing magnification factor. The observed line luminosity also requires a minimum mass of  $\sim 2 \times 10^8 \left(\frac{10}{\mu}\right) M_{\odot}$  in ionized gas, that is 0.33% of the estimated total molecular gas mass of  $6 \times 10^{10} \left(\frac{10}{\mu}\right) M_{\odot}$ . We compile multi-band photometry tracing rest-frame ultraviolet to millimeter continuum emission to further constrain the properties of this dusty high-redshift, star-forming galaxy. Via SED modeling we find G12v2.43 is forming stars at a rate of  $916 \left(\frac{10}{\mu}\right) M_{\odot}$  yr<sup>-1</sup> and already has a stellar mass of  $8 \times 10^{10} \left(\frac{10}{\mu}\right) M_{\odot}$ . We also constrain the age of the current starburst to be  $\leqslant 5$  Myr, making G12v2.43 a gas-rich galaxy lying above the star-forming main sequence at  $z \sim 3$ , undergoing a growth spurt, and it could be on the main sequence within the derived gas depletion timescale of  $\sim 66$  Myr.

*Key words:* galaxies: high-redshift – galaxies: individual (G12v2.43) – galaxies: starbursts – galaxies: stellar content – instrumentation: spectrograph – submillimeter: galaxies

# 1. Introduction

Over the past 20 years, wide-field multi-band surveys have demonstrated that the star formation rate (SFR) per unit comoving volume of the universe rose quickly soon after re-ionization and peaked at redshifts between  $z \sim 3$  and 1 (look-back times of  $\sim$ 11.5 to 7.7 Gyr) at rates 10 to 15 times the present-day values (see e.g., Madau & Dickinson 2014). Locally, and even back beyond redshift 3, a substantial fraction of star formation within galaxies is obscured by dust. This dust absorbs starlight, and re-radiates its power in the far-infrared (far-IR) continuum. For most high-luminosity, star-forming galaxies, the far-IR luminosity exceeds the optical/ultraviolet (UV) luminosity so we have come to call these dusty starforming galaxies (DSFGs). DSFGs dominate the rise in SFR density looking back in time to at least beyond a redshift of 3, so it is important to study DSFGs in their rest-frame far-IR bands to properly understand the history of star formation in the universe.

We have constructed two sub-millimeter (submm) grating spectrometers, ZEUS (Hailey-Dunsheath 2009) and ZEUS-2 (Ferkinhoff et al. 2014), in order to measure far-IR fine-structure line emission from luminous star-forming galaxies between z=1–5. These far-IR lines (e.g., [C II] 158, [N II] 122 and 205, [O III] 88 and 52  $\mu$ m) are important coolants of the

gas, and excellent probes of both the physical properties of the emitting medium and the dominant sources of luminosity—a burst of star formation activity or accretion onto a supermassive black hole. They have advantages over the optical lines in that they are typically optically thin, insensitive to extinction by dust,<sup>6</sup> and for lines arising from ionized gas, they are also insensitive to the ionized gas temperature. In the local universe, a full complement of far-IR fine structure lines has been studied in many sources, helping us to constrain the properties of the interstellar medium and the host stellar populations, using airborne and space-based instruments (e.g., Brauher et al. 2008; Graciá-Carpio et al. 2011; Farrah et al. 2013; Cormier et al. 2015; Díaz-Santos et al. 2017). At z > 0.2, the sensitivity of the instruments and the Earth's atmosphere makes measurements of these lines very challenging. Using our ZEUS instruments, we survey star-forming galaxies in the redshift 1 to 5 epoch in their far-IR fine-structure line emission, including the [C II] 158  $\mu$ m line (Hailey-Dunsheath et al. 2010; Stacey et al. 2010; Ferkinhoff et al. 2014; Brisbin et al. 2015).

The far-IR lines of [O III] and [N II] arise in H II regions, and are prominent coolants tracing the physical conditions and excitation mechanism of gas in sites of active star formation.

<sup>&</sup>lt;sup>6</sup> An extinction optical depth of unity requires a gas column of  $N_{\rm H} > 10^{24} \, {\rm cm}^{-2}$  for  $\lambda \geqslant 60 \, \mu{\rm m}$  (Draine 2003).

The lines individually allow us to measure the flux of ionizing radiation, while the [O III]  $88 \,\mu\text{m}/[\text{N II}] 122 \,\mu\text{m}$  line ratio (modulo abundance considerations) is primarily sensitive to the hardness of the radiation field (e.g., Rubin 1985). Combined, these constraints provide a luminosity-weighted measurement of the number and type of the of the most massive stars still on the main sequence and hence the intensity and age of the most recent starburst (see Ferkinhoff et al. 2010). To pursue our goal of characterizing the starbursts in high-redshift DSFGs, we are surveying the [O III] 88  $\mu$ m and [N II] 122  $\mu$ m lines using our submm grating spectrometers ZEUS (on CSO) and ZEUS-2 (on APEX). Theoretical modeling of emission regions and observations of local galaxies suggest that the [N II]  $122 \mu m$ line is fainter than the [O III]  $88 \mu m$  line, and only two detections have been reported at z > 1, both in composite starburst-active galactic nucleus (AGN) systems, by (Ferkinhoff et al. 2011, 2015). To date, the [O III] 88  $\mu$ m line has only been reported in five high-redshift submm galaxies (SMGs), two detected with ZEUS, two with Herschel-SPIRE in  $z \sim 3$  lensed SMGs (Valtchanov et al. 2011; Rigopoulou et al. 2018), and one with ALMA at  $z \sim 6.9$  (Marrone et al. 2017). Three additional detections of the  $[O III] 88 \mu m$  line have been reported in clumps associated with Ly $\alpha$  systems at  $z \sim 7-8$  using ALMA (Inoue et al. 2016; Carniani et al. 2017; Laporte et al. 2017). Here, we report observations of the [O III]  $88 \,\mu\mathrm{m}$  line in a Herschel-discovered SMG, G12v2.43 at z = 3.127 with ZEUS-2 on the APEX telescope in the 350  $\mu$ m waveband.

G12v2.43 (R.A.: 11:35:26.3 decl.: -01:46:06.5, J2000) was discovered in the Herschel Astrophysical Terahertz Large Area Survey (H-ATLAS, Clements et al. 2010), and was selected as a candidate high-redshift gravitationally lensed source due to its large 500  $\mu m$  flux density ( $S_{500\mu m} > 0.1 \,\mathrm{Jy}$ ). It was confirmed as a high-redshift ( $z = 3.1276 \pm 0.0005$ ) system through mm-band spectroscopy using the Green Bank Telescope (GBT, Harris et al. 2012) and the Northern Extended Millimeter Array (NOEMA, Yang et al. 2016). These observations show powerful emission in low-J CO and H<sub>2</sub>O rotational lines, thereby confirming G12v2.43's extreme luminosity. In a high spatial resolution study, using the Submillimeter Array (SMA), Bussmann et al. (2013) reported the detection of dust continuum at (observed frame) 896  $\mu$ m. The source was marginally resolved but did not show any extended emission or obvious signatures of gravitational lensing like multiple images or lensing arcs at 0.18 (FWHM) scale. Follow-up deep near-IR imaging to find the foreground lensing galaxy by Calanog et al. (2014) detected no significant emission in the  $K_s$  band either from the foreground lens or the background high-redshift galaxy. We note that the co-ordinates reported above are the true centroid of the emission seen in the SMA map and are offset by 1"4 from the those reported in Bussmann et al. (2013).

A reasonable explanation for its extreme luminosity,  $L_{\rm IR}$ , of  $\sim 1.2 \times 10^{14} L_{\odot}$  (Bussmann et al. 2013) could be magnification due to gravitational lensing, as was suggested by Harris et al. (2012) due to the large CO luminosity and small line FWHM. For discussions related to physical quantities in this paper, we adopt a scaling factor of  $\left(\frac{10}{\mu}\right)$ , where  $\mu$  would be the true lensing magnification factor. Within the purview of existing observations, the influence of gravitational lensing

for G12v2.43 remains unconstrained. However as a reference for the reader, galaxies with such extreme observed luminosities and well constrained lensing models have a median magnification factor of  $\mu \sim 6$  (e.g., Bussmann et al. 2013; Spilker et al. 2016). If confirmed, the apparent brightness of G12v2.43 would allow future observations to study a normal galaxy building up its stellar mass at sub-kpc resolution and study the interplay between star formation and galaxy evolution only 2 Gyr after the Big Bang.

In this paper we present the [O III] 88  $\mu$ m line observations and compile broadband photometry from UV to mm wavelengths toward G12v2.43 to study the properties of its ionized gas, dust, and stellar populations. In Section 2, we present the ZEUS-2/APEX observations and discuss the constraints on its young stellar population and ionized gas mass. In Section 3, we compile new observations of G12v2.43 from various archives, namely near-IR data taken with the Hubble and Spitzer Space Telescopes and far-IR photometry and spectroscopy with the Herschel Space Observatory. In Section 4, we present spectral energy distribution (SED) modeling of the photometric data and discuss the interstellar medium (ISM) properties of G12v2.43 and the potential for it to be a gravitationally lensed system. Throughout this paper we assume a flat  $\Lambda$ CDM cosmology with a Hubble constant of  $70 \,\mathrm{km \, s^{-1} \, Mpc^{-1}}, \quad \Omega_{M} = 0.3, \quad \mathrm{and} \quad \Omega_{\Lambda} = 0.7, \quad \mathrm{giving}$ G12v2.43 a luminosity distance of 26.7 Gpc and a linear scale of 7.6 kpc arcsec<sup>-1</sup>.

#### 2. ZEUS-2/APEX Observations and Results

The second-generation redshift (z) and Early Universe Spectrometer (ZEUS-2) is a grating spectrometer optimized for detecting broad (few  $100\,\mathrm{km\,s^{-1}}$ ) spectral lines from distant galaxies as they are redshifted into the short submm telluric windows (Ferkinhoff et al. 2012; Parshley et al. 2012; Ferkinhoff et al. 2014). We observed G12v2.43 with ZEUS-2 at the APEX telescope (Güsten et al. 2006) in 2014 October under very good weather conditions. The telescope was pointed at the coordinates reported in Bussmann et al. (2013), offset by 1.14 from the peak of the submm emission, but well within the ZEUS-2/APEX beam. The precipitable water vapor remained stable between 0.5 and 0.56 mm, which corresponds to a line-of-sight transmission of 31%–42% at  $365\,\mu\mathrm{m}$  during the course of the observations.

The [O III] 88  $\mu$ m line was observed at 364.7  $\mu$ m based on the redshift reported by Harris et al. (2012). The resolving power of the instrument at 365  $\mu$ m (in the fifth order of the echelle grating) is  $R \sim 960$ . Each spectral pixel covers  $\sim 313 \, \mathrm{km \, s^{-1}}$  in velocity space with the array providing an instantaneous coverage of  $\sim$ 3500 km s<sup>-1</sup>. Data were taken in standard chop/nod mode, with 2 Hz chop frequency and a 30" azimuthal chop-throw. The source elevation was between 50° and 68° during the observations. Three grating settings were used to move the line along spectral pixels to increase total spectral coverage and eliminate gaps due to nonfunctioning pixels. As a result, the data were sampled at  $230 \,\mathrm{km \, s^{-1}}$ , finer than our resolution element of  $313 \,\mathrm{km \, s^{-1}}$ . We obtained 8 × 10 minute integrations with a chop efficiency of 63%, giving a total on-source integration time of 25.2 minutes. Pointing and focus observations were taken on the <sup>12</sup>CO(6-5) line from IRC10216, and were repeated every 20 minutes. Pointing was found accurate to within 2" over the duration of the observations. The ZEUS-2/APEX beam at 365  $\mu$ m was measured to be  $7.8'' \pm 0.9''$  using Uranus. Gain calibration for spectral

APEX (Atacama Pathfinder Experiment) is a collaboration between the Max-Planck-Institut für Radioastronomie, the European Southern Observatory, and the Onsala Space Observatory.

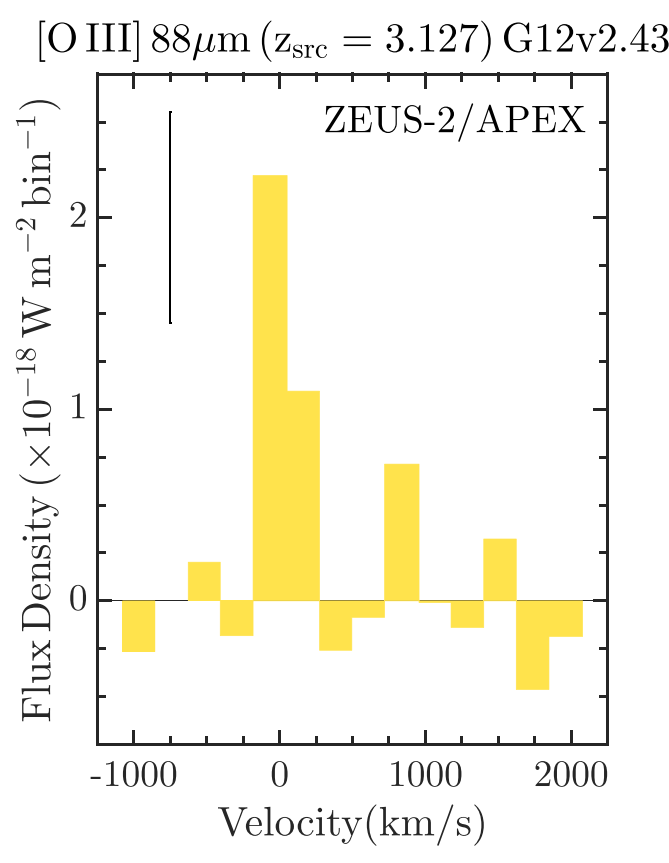


Figure 1. ZEUS-2/APEX spectrum of the [O III] 88  $\mu$ m emission line observed in G12v2.43 at a redshift of z = 3.127. The velocity scale is with respect to the source redshift. Typical per bin 1- $\sigma$  error is shown at the top left.

pixels was done by chopping an ambient temperature blackbody against the cold sky before and after each set of onsource observations and flux calibration was verified with Jupiter and Uranus. The signal we measured from Uranus indicated that the point source coupling for APEX was  $\sim 40\%$  at 365  $\mu$ m. We detected the [O III]  $88 \,\mu\mathrm{m}$  line, shown here in Figure 1, at a flux level of  $3.2 \pm 0.4 \times 10^{-18} \, \mathrm{Wm^{-2}}$  (S/N =7.5), or equivalently 116  $\pm$  15 Jy km s<sup>-1</sup>, with an estimated calibration uncertainty of 30%. We advise the reader to use the velocity FWHM of 225 km s<sup>-1</sup>, derived by spectrally resolved observations of Harris et al. (2012) and Yang et al. (2016) for the CO and H<sub>2</sub>O lines respectively, to estimate the peak line flux density.

# 2.1. [O III] Line Emission: Young Stars and Ionized Gas Mass

As the O<sup>++</sup> ion requires 35 eV to form, it indicates the presence of a very hard ionizing source which could either be upper main sequence stars, with effective temperature >36,000, in the vicinity of the emitting region or a nearby AGN. Assuming the star formation-dominated scenario, the [O III] line emission can be used to constrain the type of stars producing the ionizing radiation (O8 or hotter) and the line luminosity can be used to estimate the flux of ionizing photons required to support the observed emission. Using theoretical models for upper main sequence stars, we can scale the number of ionizing photons produced by a certain spectral type of O-star to estimate the number of such stars present, on average, in the host galaxy. Also, since the most massive stars spend a relatively short amount of time on the main sequence, up to about 3-10 Myr, the observed [O III] line emission places a constraint on the age of the most recent starburst.

Our observations of the [O III] 88  $\mu m$  line flux correspond to a luminosity of  $7.1 \times 10^9 \left(\frac{10}{\mu}\right) L_{\odot}$  at the distance of G12v2.43. In Section 4.1, we suggest that the emission seen from G12v2.43 is dominated by star formation activity and not from an AGN with the help of broadband SED modeling. With the [O III] line flux, we can constrain the number of photons capable of doubly ionizing oxygen, and estimate the number of O-stars given an upper mass cutoff. We use the H II region models of Rubin (1985) to scale the observed line flux and estimate the number of Lyman continuum photons. The effective stellar temperatures,  $T_{\rm eff}$ , used in the models are matched with those of the spectral type of main sequence Ostars using the calibration of Martins et al. (2005). The main sequence lifetime is based on the hydrogen burning timescale reported by Ekström et al. (2012) for massive stars of solar metallicity. We use Rubins K models which are based on stellar atmosphere models from Kurucz (1979, 1993) with an [O/H] abundance of  $6.76 \times 10^{-4}$ , to predict the [O III] line luminosity as a function of the effective stellar temperature of the star  $(T_{\rm eff}=31-45~{\rm kK})$ , the Lyman continuum (LyC) photon rate  $(Q_0=10^{49-50}~{\rm s}^{-1})$ , and the electron number density in the H II regions  $(n_{\rm e}=10^{2-4}~{\rm cm}^{-3})$ . The models are set up such that the line intensities scale linearly for models with varying  $Q_0$ , so that the derived number of stars for the model with  $Q_0 = 10^{49} \,\mathrm{s^{-1}}$  would be 10 times the number of stars derived for models with  $Q_0 = 10^{50} \,\mathrm{s^{-1}}$ . The models with  $n_e = 10^3 \,\mathrm{cm^{-3}}$  and  $T_{\rm eff} = 40,000$  and 45,000 K provide the best fit with the derived LyC photon rate,  $Q_0 \approx 5.7 \times 10^{55} \left(\frac{10}{\mu}\right) \text{s}^{-1}$ . This LyC flux level requires (1.2–5.2)  $\times$  10<sup>6</sup> $\left(\frac{10}{\mu}\right)$  O3V to O5.5V stars. An estimate using the total bolometric luminosity of such upper main sequence stars present in the galaxy suggests that if all their starlight were absorbed by dust and re-radiated in the far-IR, that

could account for  $(0.8-1.3) \times 10^{12} \left(\frac{10}{\mu}\right) L_{\odot}$ , i.e., ~12% of the

observed far-IR luminosity of  $8.3 \times 10^{12} \left(\frac{10}{\mu}\right) L_{\odot}$ . Following Ferkinhoff et al. (2010), in the high-density, hightemperature limit, we can estimate the minimum mass ionized nebula required to support the luminosity of the observed [O III] line as:

$$M_{\min}^{\text{H}^+} = 4\pi d_{\text{L}}^2 \frac{F_{\text{O III}}}{\frac{g_l}{g_c} A_{ul} h \nu_{ul}} \frac{m_{\text{H}}}{\xi_{\text{O}^{++}}}.$$
 (1)

Here,  $F_{O \text{ III}}$  is the observed line flux (W m<sup>-2</sup>),  $d_{L}$  is the luminosity distance (m),  $g_l$  is the statistical weight (2J+1) for the J=1 emitting level,  $g_t = \sum_i g_i e^{-\Delta E_i/kT}$ , is the partition function,  $A_{ul}$  is the spontaneous emission coefficient (s<sup>-1</sup>), h is the Planck constant (J-s),  $\nu_{ul}$  is the rest frequency of the line, 3393.00624 GHz (88.356  $\mu$ m),  $m_{\rm H}$  is the mass of a hydrogen atom, and  $\xi_{O^{++}}$ , is the relative abundance of  $(O^{++}/H^+)$ . Adopting a nebular gas phase abundance,  $[O/H] = 5.9 \times$  $10^{-4}$  and assuming all the oxygen is doubly ionized  $([O/H] = [O^{++}/H^{+}])$ , we find that the minimum ionized gas mass in G12v2.43 is  $(2.0\pm0.3)\times10^8\left(\frac{10}{\mu}\right)M_{\odot}$ . The minimum mass of doubly ionized oxygen itself is  $\sim 1.9 \times 10^6$ 

Table 1
Photometry Data

Wavelength	Frequency	Flux Density	Instrument
(µm)	(GHz)	(mJy)	
1.15	260689.1	$0.9 \pm 0.2 \times 10^{-3}$	HST/WFC3
3.4	88174.3	$29 \pm 6 \times 10^{-3}$	wise/W1
3.6	83275.7	$31\pm3\times10^{-3}$	Spitzer/IRAC1
4.5	66620.5	$45 \pm 4 \times 10^{-3}$	Spitzer/IRAC2
4.6	65172.3	$31 \pm 11 \times 10^{-3}$	WISE/W2
12	24982.7	< 0.49	WISE/W3
22	13626.9	< 3.9	WISE/W4
70	4282.7	$19 \pm 3$	Herschel/PACS
100	2997.9	$56 \pm 6$	Herschel/PACS
160	1873.7	$180 \pm 12$	Herschel/PACS
250	1199.2	$296\pm17$	Herschel/SPIRE
350	856.5	$306 \pm 24$	Herschel/SPIRE
500	599.6	$214\pm23$	Herschel/SPIRE
896	334.6	$50 \pm 3$	SMA
1064	281.8	$36.4 \pm 0.3$	NOEMA
1252	239.4	$22.5\pm0.5$	NOEMA
208900	1.435	< 0.36	VLA/FIRST

**References.** The SMA photometry was previously presented in Bussmann et al. (2013); note the change in center wavelength from 880  $\mu$ m to 896  $\mu$ m. The NOEMA mm-wave photometry is adopted from Yang et al. (2016). **Note.** Wavelength/frequency in observed frame; all upper limits are 3- $\sigma$ .

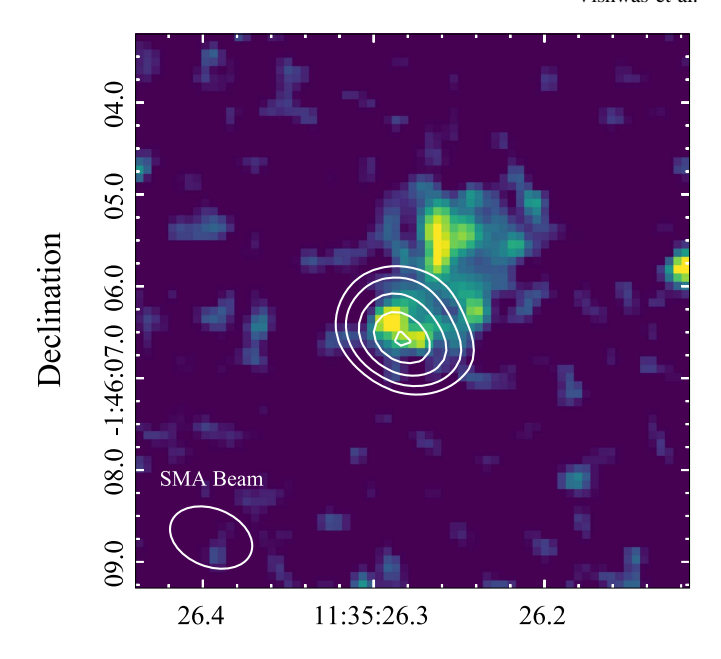
# 3. Supporting Observations

Previous observations of G12v2.43 have been reported by Harris et al. (2012), Bussmann et al. (2013), and Yang et al. (2016). However, these authors only discuss emission at wavelengths longer than (observed frame) 200  $\mu$ m, so that many of the source properties, including the stellar mass and the total luminosity, are not well constrained. We compile published and archival observations to produce a rest-frame near-UV to mm SED which we use to constrain the star formation history (SFH), stellar mass, total luminosity, and dust properties. As the source is compact and the beams of the various instruments vary from 0."15–35", flux densities (or limits) were derived via aperture photometry in the recommended manner for each instrument assuming a point source. These data are summarized in Table 1.

### 3.1. Archival: Hubble Space Telescope

As part of a snapshot program to identify gravitationally lensed galaxies (PI: Negrello, ID: 12488), G12v2.43 was observed with the *HST* Wide-field Camera (WFC3) using the wide near-IR filter F110W for 711.7 s in 2013 July. In a lensing system, the near-IR images are typically used to identify the foreground lensing galaxy and the rest frame near-UV to optical light tracing stellar emission in the background higher-redshift galaxy. We obtained the pipeline-calibrated images from the *Hubble* Legacy Archive to investigate the presence of either a foreground galaxy, or any structure like arcs or an Einstein ring, that could be characteristic of strong gravitational lensing.

We identify a source in the near-IR WFC3 F110W image at  $5.1-\sigma$  significance that is consistent with the centroid of the emission seen from the high-z galaxy in interferometric observations from SMA (Figure 2). The emission is faint  $(m_{AB} = 24.2)$ , and another source is seen 1" north-west of the location of the high-z galaxy. Previous attempts at identifying



# Right Ascension

**Figure 2.** Background: color map: a  $6'' \times 6''$  stamp of 1.1  $\mu$ m WFC3 image at the position of G12v2.43. The emission in the HST/WFC3 image shows two sources near the expected high-z source location, separated by  $\sim 1''$ . Foreground: white contours: 896  $\mu$ m continuum emission detected at the position of G12v2.43 with the SMA (from Bussmann et al. 2013). The contours, starting from the center, show the peak of the emission detected at 24- $\sigma$  and moving out to (17, 12, 8.5, 6)- $\sigma$  levels. The white ellipse in the bottom-left corner indicates the beam size of the SMA observations (FWHM:  $0''/93 \times 0''/63$ ).

the foreground lensing galaxy in the  $K_s$  band using deep Keck observations have been unsuccessful (Calanog et al. 2014), and we cannot say with certainty whether these two sources are actually patchy emission in the rest-frame near-UV from G12v2.43 or could be partially attributed to a foreground, perhaps lensing, galaxy. As the emission is extended around the two features, to estimate the flux density of the high-z source we perform photometry with a 1" circular aperture centered at the peak of the SMA emission to avoid picking up flux from the nearby source and subtract the median sky from each pixel.

# 3.2. Archival: Spitzer Space Telescope

We obtained the pipeline calibrated images of G12v2.43 from the Spitzer Heritage Archive. The source was observed using the Spitzer Infrared Array Camera (IRAC) in Cycle 11 (PI: A. Cooray, Program ID 80156) in the 3.6 and 4.5  $\mu$ m bands. The on-source integration time was 706 s. Emission in the IRAC bands traces near-IR light from the high-redshift source at the effective rest-frame wavelength of 872 nm and 1090 nm. We find bright emission in both bands at the source location, consistent with the HST F110W image reported in the previous section and with the interferometric SMA imaging, and no signs of extended emission or artifacts. We perform photometry on the Level2 pipeline products (postBCD) following the methodology described in Appendix B of the IRAC instrumentation handbook. Since the data are undersampled and there is no clear evidence for extended emission at the IRAC resolution, we perform source fitting and aperture photometry in the recommended manner using both a 3."6 and

6" aperture to estimate the flux density. The uncertainties are estimated from the uncertainty image provided with the science data products from the archive and compared to the background estimated using a large annulus around the source. The uncertainty derived from the uncertainty maps is smaller than the 5% calibration accuracy of IRAC, but the difference between various size apertures is larger, about 10%. We quote this 10% uncertainty for both of the measured flux densities for G12v2.43.

# 3.3. Archival: Widefield Infrared Survey Explorer

We utilized the publicly available all-sky data release from the *Wide-field Infrared Survey Explorer (WISE)* (Wright et al. 2010) to look for emission from G12v2.43 between 3.4 and 22  $\mu$ m. We queried the AllWISE point source catalog for entries within 5" of the *Spitzer* position. The source was only detected (5- $\sigma$ ) in W1 (3.35  $\mu$ m) band and we derived 3- $\sigma$  upper limits for the flux density in the W2 (4.6  $\mu$ m), W3 (11.56  $\mu$ m) and W4 (22.1  $\mu$ m) bands based on the magnitudes reported in the catalog; see Table 1.

#### 3.4. Archival: Herschel Space Observatory

#### 3.4.1. Photometry

Due to the redshift of G12v2.43 (z = 3.127), the mid-IR part of the SED, which could help constrain emission from a hot dust component or an obscured AGN, is shifted into the far-IR bands covered by the PACS and SPIRE instruments on board the *Herschel Space Observatory*.

We present observations of G12v2.43 taken in the 70, 100, and 160 µm bands of the PACS photometer (Poglitsch et al. 2010). The observations used here were taken as a part of the observing programs, OT1\_rivison\_1, Observation ID: 1342224173,74, on OD 792 and OT2\_jwardlow\_2, Observation ID: 1342257109-112, on OD 1309. The source was observed for 276–558 s in each band. These data were processed using HIPE version 15 (Ott 2010) through pipeline version 14.2. We combined all the observations of G12v2.43 in each PACS band and then performed point-source aperture photometry using the task sourceExtractorSussextractor. We detected the source in all three PACS bands. The flux density derived in the 160  $\mu$ m band is lower by 17% than the value reported by Wardlow et al. (2017) but consistent with that reported in the PACS point source catalog (Marton et al. 2017). The statistical error in the measurement was calculated by estimating the noise level in the map in each band. The SPIRE bands span across the peak of the dust emission at  $z \sim 3$  and are critical to estimating dust properties and the far-IR luminosity. We used the flux density reported in the SPIRE point source catalog (Schulz et al. 2017) at the location of G12v2.43. The multiplicative color correction required for the SPIRE data points is 1.02 at 250  $\mu$ m, 0.97 at 350  $\mu$ m and 0.95 at 500  $\mu$ m. In Table 1, the errors reported with the SPIRE flux densities are the confusion noise in the maps as reported by the point source catalog. The confusion noise is much larger than the 5% calibration uncertainty or the statistical noise derived by the sourceExtractorTimeline task in HIPE (2%-3%).

#### 3.4.2. Spectroscopy

G12v2.43 was observed with the SPIRE Fourier Transform Spectrometer (Griffin et al. 2010). The observations used here

 Table 2

 Far-IR Fine-structure Lines in PACS/SPIRE Observations

Line ID	Rest Wavelength (µm)	Line Flux, $3-\sigma$ ( $10^{-17} \text{ W m}^{-2}$ )
$O[O IV] ^{2}P_{3/2} \rightarrow ^{2}P_{1/2}$	25.91	<0.7ª
$[O III] {}^{3}P_{2} \rightarrow {}^{3}P_{1}$	51.81	< 0.6
[N III] ${}^{2}P_{3/2} \rightarrow {}^{2}P_{1/2}$	57.34	< 0.7
[O I] ${}^{3}P_{1} \rightarrow {}^{3}P_{2}$	63.18	< 0.6
$[O III] {}^{3}P_{1} \rightarrow {}^{3}P_{0}$	88.36	< 0.8
[N II] ${}^{3}P_{2} \rightarrow {}^{3}P_{1}$	121.89	< 0.8
[O I] ${}^{3}P_{0} \rightarrow {}^{3}P_{1}$	145.53	<1.1
[C II] ${}^{2}P_{3/2} \rightarrow {}^{2}P_{1/2}$	157.74	<1.4

#### Note.

were taken as a part of the observing program OT1\_rivison\_1, Observation ID: 1342247744, on OD 1150 in high-resolution mode for 13,752 s toward the end of the Herschel mission. We reprocessed the data through HIPE 15 with SPIRE calibration version 14.3 and corrected for instrumental artifacts. The spectral shape and absolute flux calibration were verified by comparing the SPIRE photometry with synthetic measurements derived from the corrected spectral data, using the task spireSynthPhotometry within HIPE 15. The inherent instrument response of a Fourier Transform Spectrometer is a sinc function, which has 20% sidelobes associated with each peak. Instead of looking at a single coadded scan and deriving limits for the line fluxes, we improved the noise characterization by creating multiple realizations of averaged scans by randomly selecting 100 out of the 200 available scans. As only half of the available scans were used in each realization, the sensitivity in each scan would, in principle, be worse by a factor of  $\sqrt{2}$ . From these realizations, we estimated the noise in a 5 GHz band centered at the frequency of individual far-IR lines. No lines were detected at high significance and the 3- $\sigma$  limits are listed in Table 2. We discuss the astrophysical significance of upper limits derived for the [O III] 52  $\mu$ m and the [C II] 158  $\mu$ m

The electronic ground state of doubly ionized oxygen is split by fine-structure interactions into three levels, ground  $({}^{3}P_{0})$ , and two excited states,  ${}^{3}P_{1}$ , and  ${}^{3}P_{2}$ . As the fine-structure states are only a few hundred K above the ground state, ions can be collisionally excited by free electrons in the HII regions (typical temperature  $\sim 8000 \, \mathrm{K}$ ), to occupy these states. The 3- $\sigma$ limit for the upper transition,  ${}^3P_2 \rightarrow {}^3P_1$  at 52  $\mu$ m, of  $L_{\rm [O\,III]} < 6.1 \times 10^{-18} \ {\rm W\,m^{-2}}$ , in conjunction with our detection of the ground state transition,  ${}^{3}P_{1} \rightarrow {}^{3}P_{0}$  at 88  $\mu$ m, allows us to constrain the density of the emitting gas by comparing the observed line ratio to the theoretical line emissivity ratio (Rubin 1989). The luminosity ratio of the two [O III] lines,  $\frac{\hat{L}_{[O~III]~52~\mu m}}{} < 1.92$ , suggests that the emitting gas has density  $n < 610 \,\mathrm{cm}^{-3}$ . This is consistent with our choice of H II region models with density  $n = 10^{2-3} \,\mathrm{cm}^{-3}$ , used to interpret the [O III] 88  $\mu$ m line emission in Section 2. Similarly, the 3- $\sigma$  limit for the the [C II] 158  $\mu$ m line flux,  $L_{C II} < 1.4 \times 10^{-17} \, \text{W m}^{-2}$ , yields a [C II]/far-IR luminosity ratio ≤0.4%, consistent with the ratio observed in other DSFGs at  $z \sim 1-5$ . (e.g., Stacey et al. 2010; Gullberg et al. 2015).

<sup>&</sup>lt;sup>a</sup> Line flux limit from Wardlow et al. (2017).

#### 4. Discussion

In order to understand the SFH and properties of the stellar populations and the ISM of G12v2.43, we address the observed properties of the source in the context of synthesized star formation models, and dust emission and SED models.

#### 4.1. UV-to-mm SED

Leveraging the broadband coverage we have compiled here for G12v2.43, we perform SED fitting using CIGALE (Code Investigating GALaxy Emission; Noll et al. 2009; Serra et al. 2011) and the high-z extension of MAGPHYS (Multiwavelength Analysis of Galaxy Physical Properties; da Cunha et al. 2008, 2015) with all available photometric data points described in Section 3. As the search for a lensing galaxy has been unsuccessful (Calanog et al. 2014), it is conceivable that the near-IR emission seen in the HST and IRAC maps is at least in part from the high-z galaxy. As mentioned in Section 3.1, to estimate the flux density at 1.15  $\mu$ m, we only use the emission co-incident with the centroid of the emission seen in the SMA observations. As the *Spitzer*/IRAC beam is big enough to contain emission from the nearby source, for the purpose of SED modeling we assign an error of 50% on the flux density at 3.6 and 4.5  $\mu$ m.

CIGALE builds up galaxy SEDs from UV to radio wavelengths assuming a combination of modules. These allow us to model the SFH, the stellar emission using population synthesis models (Bruzual & Charlot 2003; Maraston 2005), nebular lines, dust attenuation (e.g., Calzetti et al. 2000), dust emission (e.g., Draine & Li 2007; Casey 2012), contribution from an AGN (e.g., Fritz et al. 2006; Dale et al. 2014), and radio emission. The SEDs are built while maintaining consistency between UV dust attenuation and far-IR emission from the dust. To model the SFH, we employ a delayed SFH prescription used to model high-z star-forming galaxies (e.g., Ciesla et al. 2016) along with the dust attenuation model from Calzetti et al. (2000), and the dust emission models from Draine & Li (2007). Finally, CIGALE performs a probability distribution function analysis for our specified model parameters, and obtains the likelihoodweighted mean value for each parameter.

MAGPHYS uses a Bayesian approach to constrain galaxy-wide physical properties, including the SFR, stellar and dust masses, and contributions from both hot and cold dust components of the ISM. It builds a large library of reference spectra with different SFHs (using stellar population synthesis models from Bruzual & Charlot 2003) and dust attenuation properties (using models from Charlot & Fall 2000). Similar to CIGALE, it also ensures energy balance between the optical and UV extinction and the far-IR emission. Both CIGALE and MAGPHYS have internal filter libraries that use instrumental response curves to perform color correction.

However, the MAGPHYS package does not allow for a possible AGN contribution to the overall SED fit. In order to explore the presence of a hidden AGN in G12v2.43, we used the AGN module in CIGALE with templates from Fritz et al. (2006) to estimate a parameter that constrains the fraction of observed emission that could be due to an AGN. We compare the resulting best-fit models and derived parameters from both CIGALE and MAGPHYS. We find that the AGN contribution is negligible in G12v2.43 and the observed SED is well explained by a dust-obscured starburst. For such a heavily obscured system, extinction due to a large column of dust may

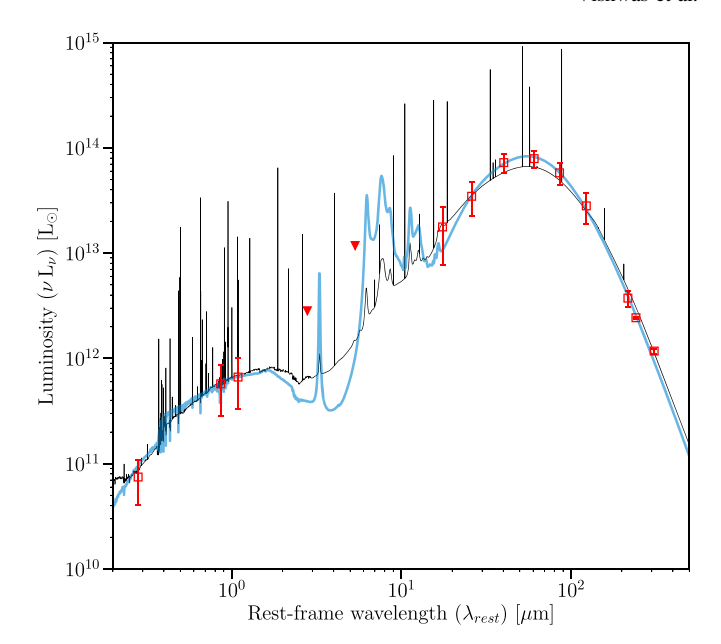


**Figure 3.** Spectral energy distribution fit for G12v2.43 using broadband photometry with CIGALE (black) and MAGPHYS (blue). The red squares are the input photometry measurements with associated error bars. The red solid triangles indicate the upper limits derived from the *WISE* W3 and W4 bands.

lead to corrections that could be important for deriving physical properties (e.g., Uzgil et al. 2016). Using a modified blackbody approximation for the dust emission, we estimate the wavelength  $\lambda_0 = c/\nu_0$  where the optical depth  $\tau_{\nu} = (\nu/\nu_0)^{\beta}$ reaches unity for G12v2.43. In doing so, we make the following assumptions: the resolved dust continuum size from the SMA observations is used to measure the source solid angle, the dust emissivity spectral index  $\beta$  is fixed to 1.5, and the correction due to contrast against the cosmic microwave background (CMB) is negligible. We find  $\lambda_0^{\rm rest} = 32 \pm 8 \,\mu{\rm m}$ and, assuming the dust is well mixed in the medium, the correction to the reported [O III]  $88 \,\mu\mathrm{m}$  line luminosity in Section 2 would be  $\sim$ 11%, well within the reported uncertainty. The SEDs and their best fits from both CIGALE and MAGPHYS are plotted in Figure 3. Both SED fits are consistent within the errors and the corresponding best-fit parameters are listed in Table 3.  $L_{\rm IR}$  is calculated by integrating under the bestfit SED between  $\lambda_{\mathrm{rest}} = 8\text{--}1000\,\mu\mathrm{m}$  and  $L_{\mathrm{FIR}}$  by integrating over  $\lambda_{\rm rest} = 42.5 - 122 \,\mu{\rm m}.$ 

#### 4.2. Constraining the Stellar Population

We showed in Section 2.1 that, assuming the [O III] line emission we detect in G12v2.43 arises from H II regions formed by stars, then the young stellar population likely contains  $5 \times 10^6 \left(\frac{10}{\mu}\right)$  upper main sequence stars. In 4.1, with the help of the broadband SED, we find that indeed the luminosity of the source is dominated by star formation activity and argue against the presence of an AGN. Also, as a part of the SED modeling exercise, we build a stellar population model to constrain the SFR and stellar mass. The best-fit models suggest a stellar mass content of G12v2.43 to be  $7.7 \times 10^{10} \left(\frac{10}{\mu}\right) M_{\odot}$  with about 12% of that mass attributed to an ongoing starburst event with an average SFR =  $916 \left(\frac{10}{\mu}\right) M_{\odot}$  yr<sup>-1</sup>. As mentioned in Section 4.1, the uncertainty of assigning the flux from Spitzer/IRAC photometry to the high-redshift source

**Table 3**Derived Physical Properties of G12v2.43

Quantity	Value	Unit	Notes/Ref
Stellar Mass $(M_{\star})$	$7.7^{+1}_{-4} \times 10^{10}$	$\left(\frac{10}{\mu}\right) M_{\odot}$	(1)
IR Luminosity ( $L_{\rm IR}$ )	$1.3\pm0.1\times10^{13}$	$\left(\frac{10}{\mu}\right)L_{\odot}$	$(1), (2)^{\mathbf{a}}$
Far-IR Luminosity ( $L_{FIR}$ )	$8.3 \pm 0.9 \times 10^{12}$	$\left(\frac{10}{\mu}\right)L_{\odot}$	$(1), (3)^{\mathbf{b}}$
[O III] $_{88}$ Luminosity ( $L_{ m OIII}$ )	$7.1 \pm 0.9 \times 10^9$	$\left(\frac{10}{\mu}\right)L_{\odot}$	(4)
Dust Temperature ( $T_{\text{dust,MBB}}$ )	$49.6_{-3.6}^{+5.6}$	K	(1)
Dust Temper- ature ( $T_{\text{dust,Draine}}$ )	34 ± 1	K	(5)
Star Formation Rate (SFR)	$916^{+88}_{-206}$	$\left(\frac{10}{\mu}\right)$	(1)
Dust Mass (M <sub>dust</sub> )	$5.4 \pm 0.9 \times 10^8$	$M_{\odot} \text{ yr}^{-1} \ \left(\frac{10}{\mu}\right) M_{\odot}$	(1)
Ionized Gas Mass $(M_{\min}^{H^+})$	$2.0 \pm 0.3 \times 10^8$	$\left(\frac{10}{\mu}\right) M_{\odot}$	(4)
Ionized Gas Density $(n_{H^+})$	<610	$\mathrm{cm}^{-3}$	(4)
Molecular Gas $Mass (\alpha_{CO} = 0.8)$	$1.2 \pm 0.7 \times 10^{10}$	$\left(\frac{10}{\mu}\right) M_{\odot}$	(2)
Molecular Gas Mass (Genzel et al. 2015)	$6.1 \pm 0.7 \times 10^{10}$	$\left(\frac{10}{\mu}\right)M_{\odot}$	(6)

**Notes.** (1) This work, parameter derived from best-fit SED with MAGPHYS; (2) Harris et al. (2012); (3)  $L_{\rm FIR} = 8.9 \times 10^{13} \, L_{\odot}$  (<sup>b</sup>), Wardlow et al. (2017); (4) this work, based on [O III] 88  $\mu$ m line emission reported in Section 2.1 and discussion in Section 3.4.2; (5) this work, based on  $U_{\rm min} = 24$ , from CIGALE dust emission best-fit model; (6) this work, based on the method outlined by Genzel et al. (2015) using a variable metallicity dependent  $\alpha_{\rm CO}$ .

dominates the errors in determining the total stellar mass as reported in Table 3. We also find that the predicted [O III] 88  $\mu$ m line luminosity from the nebular emission component of the best-fit model,  $L_{\rm [O~III]} = (10 \pm 4) \times 10^9 \left(\frac{10}{\mu}\right)$   $L_{\odot}$  is in agreement with the observed line luminosity reported in Section 2.1, adding confidence to our interpretation that G12v2.43 hosts a significant young stellar population.

Another way to look at the number and mass of the upper main sequence stars is to estimate them using an initial mass function (IMF) assuming an SFR. Here, we assume a Salpeter IMF of the form  $\Phi(M) \propto M^{-2.35}$  with an upper mass cutoff of  $100\,M_\odot$  and a lower mass cutoff of  $1\,M_\odot$ . In a continuous star formation scenario, the equilibrium number for O-stars with mass  $>34.4\,M_\odot$  (O5.5 or higher) could be estimated as follows.

Total *mass* of stars formed in an year = SFR,

SFR = 
$$\int_{1}^{100} M \times k \ M^{-2.35} \ dM$$
. (2a)

Here k is an arbitrary constant of proportionality:

$$\Rightarrow k = \frac{\text{SFR}}{\int_{1}^{100} M^{-1.35} dM} = \frac{\text{SFR}}{2.287}.$$
 (2b)

Total number of stars formed per year with  $M > M_{low}$ ,

# of Stars, 
$$N = \int_{M_{low}}^{100} k \ M^{-2.35}$$
. (2c)

If the main sequence lifetime of a star with mass  $M_{low}$  is  $\tau_{MS}$ , then its equilibrium number would be

$$N_{\rm Eq} \approx \frac{\rm SFR}{2.287} \int_{M_{\rm low}}^{100} M^{-2.35} \times \tau_{\rm MS}.$$
 (2d)

For an O5.5 star, where its main sequence lifetime is  $\tau_{\rm MS} = 4.9\,{\rm Myr}$  (Ekström et al. 2012), the equilibrium number of O5.5 or higher stars in a continuous star formation scenario with an SFR = 916  $M_{\odot}\,{\rm yr}^{-1}$  would be  $\sim$ (916/2.287)  $\times$  4.76  $\times$  10<sup>-3</sup>  $\times$  4.9  $\times$  10<sup>6</sup> = 9.3  $\times$  10<sup>6</sup> or about twice the current number. This simple result demonstrates that the star formation event, if sustained at its present rate, must be less than 5 Myr old.

Starburst99 models (Leitherer et al. 1999) for continuous star formation utilize the same constraints and provide an independent comparison for the quantities derived here. The Starburst99 models count the number of O-stars as those with  $T_{\rm eff} > 30,000$  K, which would correspond to all stars above  $\sim 15.6~M_{\odot}$  (Martins et al. 2005). But a star of spectral class O5.5 or earlier has a mass  $M > 34.4~M_{\odot}$ , and such stars account for only about 28% of the total number of stars considered to be O-stars by the Starburst99 models. In the continuous star formation scenario forming  $1~M_{\odot}~\rm yr^{-1}$ , Starburst99 reports 20,800 O-stars after 4.9 Myr. To get the estimated number of O-stars,  $(5 \times 10^6/0.28) \sim 1.8 \times 10^7$ , the Starburst99 models would require an effective SFR of 859  $M_{\odot}~\rm yr^{-1}$ , which is consistent with our estimated SFR of 916  $M_{\odot}~\rm yr^{-1}$  within errors.

## 4.3. Conditions of Interstellar Gas and Dust

Here we will compare the interstellar dust and gas content of G12v2.43 using available data, particularly gas mass reported by Harris et al. (2012) using <sup>12</sup>CO(1–0) line observations, the dust mass estimate from the SED, and the molecular gas mass estimates using the method described in Scoville et al. (2016) and Genzel et al. (2015). The continuum measurements on the Rayleigh-Jeans (R-J) tail can be used to independently estimate total molecular gas mass using the method described in Scoville et al. (2016). The main caveat for using the continuum to derive molecular gas mass estimates using this technique is that the continuum data point should be well on the R-J tail and not near the peak of the dust blackbody emission. Here, we only use the continuum points longward of 890  $\mu$ m (observed frame) or >210  $\mu$ m rest-frame at z=3.127 (see Table 1). We use the relationship between total molecular gas mass in the galaxy and continuum flux density observed on the R-J tail by Scoville et al. (2016):

$$M_{\text{mol}} = 1.78 \left( \frac{S_{\nu}}{\text{mJy}} \right) \left( \frac{d_L}{\text{Gpc}} \right)^2 \left( \frac{\nu_{\text{obs}}}{\nu_{850 \,\mu\text{m}}} \right)^{-3.8}$$

$$\times (1 + z)^{-4.8} \left( \frac{\Gamma_0}{\Gamma_{\text{RI}}} \right) 10^{10} \, M_{\odot}, \tag{3a}$$

where, 
$$\Gamma_{RJ}(z, T_d, \nu_{obs}) = \frac{h\nu_{obs}(1+z)/kT_d}{e^{h\nu_{obs}(1+z)/kT_d} - 1}$$
,  
and,  $\Gamma_0 = \Gamma_{RJ}(0, 25 \text{ K}, \nu_{850 \mu m}) = 0.7$ . (3b)

It has often been suggested that the temperature of the cold dust component in galaxies derived using modified blackbody models tends to be biased higher when compared to the

<sup>&</sup>lt;sup>a</sup> In both cases the IR luminosity is calculated between 8 and 1000  $\mu$ m.

 $<sup>^{\</sup>rm b}$   $L_{\rm FIR}$  reported by (3) based on luminosity integrated over 40–500  $\mu{\rm m}.$ 

expected temperature of the bulk of the dust mass present in the ISM (e.g., Draine & Li 2007; Scoville et al. 2016). As part of the SED modeling we used the dust models from Draine & Li (2007) to constrain the distribution of the ambient interstellar radiation field intensity (U). The models further estimate an average dust temperature based on the minimum intensity of radiation field as  $T_{\rm dust} = 20~{\rm U}_{\rm min}^{1/6}~{\rm K}$  (Draine 2011), which for G12v2.43 results in  $T_{\rm dust} = 34~{\rm K}$  based on  $U_{\rm min} = 24 \pm 4$ . In order to be closest to the calibration derived by Scoville

et al. (2016), we use the above dust temperature along with the

896  $\mu$ m continuum observations in Equation 3(a) to estimate the molecular gas mass in G12v2.43 to be  $M_{mol} = 1.8 \times 10^{11}$  $\left(\frac{10}{\mu}\right)M_{\odot}$ . For comparison, Harris et al. (2012) reported a total molecular gas mass,  $M_{\rm mol} = (1.2 \pm 0.7) \times 10^{10} \left(\frac{10}{\mu}\right) M_{\odot}$  based on observations of the <sup>12</sup>CO(1–0) line luminosity and assuming a CO-to-H<sub>2</sub> conversion factor,  $\alpha_{\rm CO} = 0.8~M_{\odot}$  $(K \text{ km s}^{-1} \text{ pc}^2)^{-1}$ . This choice of  $\alpha_{CO}$  is typically used for local ultra-luminous infrared galaxies (ULIRGs) and to compare molecular mass estimates between high-z SMGs. Even if we use the "luminosity-weighted" dust temperature derived from the SED fit,  $T_{\text{dust}} = 49.6 \text{ K}$  in Equation 3(a), we estimate a molecular gas mass of  $1.3 \times 10^{11} \left(\frac{10}{\mu}\right) M_{\odot}$ . We also verify that we get similarly high molecular gas mass estimates using the continuum data points reported by Yang et al. (2016) at 1 and 1.25 mm (240 and 300  $\mu$ m respectively in the rest frame of G12v2.43). We apply the appropriate correction factors  $\Gamma_{RJ}$  as defined in Equation 3(b), that account for deviation from the default calibration at 850  $\mu m$  due to redshift and dust temperature, and estimate the molecular gas mass as  $(1.6-2) \times 10^{11} \left(\frac{10}{\mu}\right) M_{\odot}$ . Therefore, using the submm dust continuum method outlined by Scoville et al. (2016), we find the estimated molecular gas mass to be 10-16 times larger than that derived using the  $^{12}CO(1-0)$  line observations with a ULIRG-like conversion factor of 0.8  $M_{\odot}$  (K km s<sup>-1</sup> pc<sup>2</sup>)<sup>-1</sup>.

We derive a total dust mass of,  $M_{\rm dust} = (5.4 \pm 1) \times 10^8$   $\left(\frac{10}{\mu}\right) M_{\odot}$  from the best-fit SED model. Genzel et al. (2015) provide a relationship to estimate the dust mass using the SFR and modified dust blackbody temperature,

$$M_{\rm dust} = 1.2 \times 10^{15} \left( \frac{\rm SFR}{M_{\odot} \, \rm yr^{-1}} \right) \left( \frac{T_{\rm dust}^{\rm MBB}}{\rm K} \right)^{-5.5} M_{\odot}.$$
 (4)

Using  $T_{\rm dust} = 49.6$  K and SFR = 916  $M_{\odot}$  yr<sup>-1</sup> in Equation (4), we find  $M_{\rm dust} = 5.1 \times 10^8$   $M_{\odot}$  which is consistent with the total dust mass derived from the best-fit SED. Now, we compare the dust-to-gas mass ratio using the different molecular gas mass estimates with a metallicity-dependent dust-to-gas ratio,  $\delta_{dg}$  from Leroy et al. (2011),

$$\log_{10} \delta_{dg} = \log_{10} \left( \frac{M_{\text{dust}}}{M_{\text{mol}}} \right) = -2 + 0.85$$

$$\times (12 + \log_{10} [\text{O/H}] - 8.67). \tag{5}$$

If we use the  $^{12}CO(1-0)$  measurement along with a ULIRG-like conversion factor, we find that G12v2.43 has a metallicity of 12+log[O/H]=9.4, whereas using the estimate of the molecular gas mass using the R-J continuum, we find a

metallicity of  $12 + \log[O/H] = 8.2$ . In contrast, using a fitting function for metallicity by combining the stellar massmetallicity relation at different redshifts as given in Equation (12) by Genzel et al. (2015), we find a metallicity of 12+log  $[{
m O/H}] = 8.6 \pm 0.1$ . Using this estimate of metallicity in Equation (5), we find  $\delta_{dg} = (0.8-1) \times 10^{-2}$ . This would imply a total molecular gas mass of  $M_{\rm mol} = 6.1 \pm 0.7 \times 10^{10} \left(\frac{10}{\mu}\right)$   $M_{\odot}$  and an implied  $\alpha_{\rm CO} \approx 4~M_{\odot}~({\rm K~km~s^{-1}~pc^2})^{-1},$  quite similar to that observed in the Milky Way. For a galaxy undergoing a vigorous starburst event of the likes we suggest for G12v2.43, the filling fraction of star-forming, denser gas could be higher than the typical local ULIRG values. Downes et al. (1993) parameterized the conversion factor,  $\alpha_{\rm CO} \propto \sqrt{n}/T_b$ , where n is the average  $H_2$  density of the gas clouds and  $T_b$  is the intrinsic brightness temperature of the <sup>12</sup>CO(1–0) line. A higher volume-averaged density of the medium could account for the relatively high  $\alpha_{CO}$  value suggested here. We use this estimate of the molecular gas mass for further discussion.

Even though the various molecular gas mass estimates vary significantly, the implied baryonic gas fraction,  $\left(f_{\rm gas} = \frac{M_{\rm mol}}{M_{\rm mol} + M_{\rm stellar}}\right)$ , is  $f_{\rm gas} = 0.44^{+0.23}_{-0.30}$ , which is similar to observed gas fractions in gas-rich, high-z SMGs (e.g., Tacconi et al. 2013, 2018). The high gas fraction and yet relatively short gas depletion timescale of 66 Myr, along with the enormous SFR, agree with our understanding of the star formation activity in G12v2.43. Specifically, that it is undergoing a star formation episode, building up its stellar mass, and is currently above the star-forming main sequence at  $z \sim 3$  (Speagle et al. 2014).

# 4.4. Is G12v2.43 Strongly Lensed?

With the high signal-to-noise, SMA continuum observations (FWHM:  $0.^{\prime\prime}93\times0.^{\prime\prime}63$ ), we derive the de-convolved source size of the dust-emitting disk as  $(0.^{\prime\prime}7\pm0.^{\prime\prime}1)\times(0.^{\prime\prime}6\pm0.^{\prime\prime}1)$ , which corresponds to a physical size of  $(5.6\times4.5)\,\mathrm{kpc}$  or  $r_{\mathrm{dust}}\sim5\,\mathrm{kpc}$ . In terms of area, this is about seven times larger than the typical size of the dust disk,  $r_{\mathrm{dust}}\sim1.8\,\mathrm{kpc}$ , found by Hodge et al. (2016) in a resolved study of sixteen  $z\sim2.5\,\mathrm{SMGs}$ . As gravitational lensing spreads the intrinsic source over a larger area, a lensing magnification factor of  $\mu\sim7\,\mathrm{could}$  make G12v2.43's dust disk consistent with those observed in other high- $z\,\mathrm{SMGs}$ .

The observed line widths for spectral lines tracing various transitions of CO and  $H_2O$  in G12v2.43 are about  $\sim\!225~{\rm km\,s^{-1}}$ . As a comparison, in a study of the J>2 CO line observation in DSFGs presented in Bothwell et al. (2013), the mean value for CO line widths was found to be  $(510\pm80)~{\rm km\,s^{-1}}$ . This might indicate that G12v2.43 is either an almost face-on disk or not an intrinsically massive galaxy. As the CO line emission has been used to study the mass and kinematics of galaxies, Harris et al. (2012) suggested that there should be a "Tully–Fisher"-like relationship between the CO line width and the intrinsic line luminosity. Based on the bright  $^{12}{\rm CO}(1-0)$  line detection and the small line width they suggested a lensing magnification factor  $\mu\sim17\pm11$  for G12v2.43.

We can also estimate the CO-emitting size, even without spatially resolved observation, assuming that the CO emission is optically thick. Following Equation (2) from Solomon &

Vanden Bout (2005),

$$L'_{\rm CO} = 1.13(T_{\rm ex} - T_{\rm CMB}(z))\Delta v_{\rm FWHM} r_{\rm CO}^2$$
 (6)

The temperature of the CMB at z=3.127 is  $T_{\rm CMB}=11.2$  K. The first rotational transition of the  $^{12}{\rm CO}$  line only lies about 5.51 K above ground and the molecules can be easily excited by the ambient radiation field and by collisions in the gas. We apply an excitation temperature of  $T_{\rm ex}=30$  K, assuming that it should be higher than the background CMB temperature and perhaps lower than the dust temperature,  $T_{\rm dust}=50$  K. Now, with the observed line luminosity,  $L'_{\rm CO}=1.5\times10^{11}$  K km s $^{-1}$  pc $^2$  and measured line FWHM,  $\Delta v_{\rm FWHM}=225$  km s $^{-1}$ , we derive a  $r_{\rm CO}=5.6$  kpc, which is about the same as the size of the dust-emitting region derived above. We note that the CO-emitting size estimate is weakly dependent on our choice of  $T_{\rm ex}$ .

For a simple rotating disk model following Neri et al. (2003), the dynamical mass of the system can be estimated as

$$M_{\rm dyn} \sin^2 i = 2.33 \times 10^5 \left(\frac{\Delta V}{{\rm km s}^{-1}}\right)^2 \left(\frac{{\rm r}}{{\rm kpc}}\right) M_{\odot},$$
 (7)

where  $i = \cos^{-1}(\frac{4.5}{5.6}) = 36.5$  is the inclination angle estimated from the resolved dust continuum,  $\Delta V$  is the CO line velocity dispersion in km s<sup>-1</sup> (=FWHM/2  $\sqrt{2 \ln 2}$ ), and r is the disk radius in kpc as derived above. We estimate the dynamical mass of the galaxy to be,  $M_{\rm dyn}=3.4\times 10^{10}~M_{\odot}$ . Since this estimate of the dynamical mass is at least two times smaller than either our estimates for the stellar mass or the gas mass, our assumption that the observed ellipticity reflects inclination is suspect. In order to make a fair comparison between the estimates of dynamical mass, molecular gas mass, and stellar mass, we need to consider how the lensing magnification factor  $(\mu)$  and the choice of CO-to-H<sub>2</sub> conversion factor  $(\alpha_{CO})$  affect our measurements. We expect the dynamical mass of the system to be larger than the estimates of either the stellar mass or the molecular gas mass. The apparent spatial size scales as  $r \propto \sqrt{\mu}$ , but the apparent luminosity (CO and stars) scales as  $L \propto \mu$ . The choice of the CO-to-H<sub>2</sub> conversion factor ( $\alpha_{CO}$ ) only changes the estimate for the molecular gas mass,  $M_{\rm mol} \propto \alpha_{\rm CO}$ . If we assume the source is unlensed (largest r,  $M_{\rm dyn}$ ) and use  $\alpha_{\rm CO}=0.8$  (lowest estimate of the molecular gas), this still results in  $M_{\rm mol} \sim 3.5 \times M_{\rm dyn}$ . Without changing the  $\alpha_{\rm CO}$  (increasing  $\alpha_{\rm CO}$  widens the discrepancy), in order to match the dynamical mass to the molecular gas mass, we would need to increase the magnification factor to  $\mu = 12.5$ . A less inclined orientation would bring the estimates closer together, but a simpler explanation for the observed line and continuum luminosities could be amplification due to the effect of gravitational lensing.

#### 5. Results and Conclusions

We have presented sensitive ground-based THz spectroscopy with ZEUS-2 at the APEX telescope, detecting the [O III] 88  $\mu$ m line in G12v2.43, a high-redshift, submm galaxy at z=3.127. The luminosity in the line is  $7.1 \times 10^9 \left(\frac{10}{\mu}\right) L_{\odot}$ , which indicates the presence of a large number of upper main sequence O-stars and allows us to constrain the number of ionizing photons available. In the high-density, high-temperature limit, we derive

that the minimum mass of ionized gas required to support the observations would be  $2.8 \times 10^8 \left(\frac{10}{\mu}\right) M_{\odot}$  or about 0.33% of the

estimated total molecular gas, 
$$M_{\rm mol} = 6.1 \times 10^{10} \left(\frac{10}{\mu}\right) M_{\odot}$$
.

The upper limit from the SPIRE spectrum on the [CII]/far-IR ratio,  $\leq 0.4\%$ , would be consistent with a compact starburst, but the small velocity width and single Gaussian profile in CO and H<sub>2</sub>O lines argue against a major merger as the source of the observed [CII]/far-IR line-to-continuum ratio. We also constrain the ionized gas density to be  $n_{\rm H^+} < 610~{\rm cm}^{-3}$  using the limit for the  $[O~III]~52~\mu m$  line from the SPIRE spectrum along with our detection of the  $[O~III]~88~\mu m$  line.

Using rest-frame UV to mm wavelength observations, we constrain a broadband SED for the source and rule out any significant contribution by an obscured AGN. We find, using both the SED and extrapolating the equivalent number of  $5 \times 10^6 \left(\frac{10}{\mu}\right)$  O5.5–O3 stars estimated using the the observed [O III] line emission, that the on-going star formation event in G12v2.43 has contributed up to 0.55-1  $\times$   $10^{10} \left(\frac{10}{\mu}\right) M_{\odot}$  to its stellar mass, i.e., up to 7%-12% of the total stellar mass,  $M_{\rm stellar} = 7.7 \times 10^{10} \left(\frac{10}{\mu}\right) M_{\odot}$ .

A gas fraction of  $f_{\rm gas} = 0.44^{+0.23}_{-0.30}$ , indicates that the galaxy has an abundant supply of gas to sustain star formation over the next 66 Myr, allowing it to effectively double its stellar mass and end up on the star-forming main sequence at  $z \sim 3$ .

We also detect rest-frame near-UV emission in the  $1.1~\mu m$  HST/WFC3 image, consistent with the centroid of the dust emission seen in the SMA 896  $\mu m$  continuum image; it appears patchy and there is another source  $\sim 1''$  away along the NE–SW axis but no obvious signature of gravitational lensing like extended arcs or an Einstein ring are seen. The apparent brightness of the galaxy suggests that it could be lensed and the low dynamical mass estimate is consistent with the lensing scenario. Higher-resolution observations are required to reveal the true nature of this otherwise apparent gargantuan, specifically to understand the role gravitational lensing plays in amplifying the observed emission and uncovering the intrinsic nature of G12v2.43.

The authors would like to thank the anonymous referee for a constructive report and suggestions that helped improve the quality of the manuscript. ZEUS-2 development and observations are supported by NSF grants AST-0705256, AST-0722220, AST-1105874, and AST-1109476, and a grant from Georgia Southern University. This publication is based on data acquired with the Atacama Pathfinder Experiment (APEX) Telescope. APEX is a collaboration between the Max-Planck-Institut für Radioastronomie, the European Southern Observatory, and the Onsala Space Observatory. The authors would like to thank the APEX staff whose excellent support helped to make this work possible. The Herschel-ATLAS is a project with Herschel, which is an ESA space observatory with science instruments provided by European-led Principal Investigator consortia and with important participation from NASA. Part of this work is based on observations made with the NASA/ESA Hubble Space Telescope, obtained from the data archive at the Space Telescope Science Institute. STScI is operated by the Association of Universities for Research in Astronomy, Inc. under NASA contract NAS 5-26555. Part of this work is also based on observations made with the Spitzer Space Telescope,

which is operated by the Jet Propulsion Laboratory, California Institute of Technology under a contract with NASA.

Facilities: APEX(ZEUS-2), HST(WFC3), Spitzer(IRAC), WISE, Herschel(PACS and SPIRE), SMA.

#### **ORCID iDs**

Amit Vishwas https://orcid.org/0000-0002-4444-8929
Carl Ferkinhoff https://orcid.org/0000-0001-6266-0213
Sarah J. U. Higdon https://orcid.org/0000-0002-4021-7453
James L. Higdon https://orcid.org/0000-0003-1397-0586
Axel Weiss https://orcid.org/0000-0003-4678-3939
Karl M. Menten https://orcid.org/0000-0001-6459-0669

#### References

```
Bothwell, M. S., Smail, I., Chapman, S. C., et al. 2013, MNRAS, 429, 3047
Brauher, J. R., Dale, D. A., & Helou, G. 2008, ApJS, 178, 280
Brisbin, D., Ferkinhoff, C., Nikola, T., et al. 2015, ApJ, 799, 13
Bruzual, G., & Charlot, S. 2003, MNRAS, 344, 1000
Bussmann, R. S., Pérez-Fournon, I., Amber, S., et al. 2013, ApJ, 779, 25
Calanog, J. A., Fu, H., Cooray, A., et al. 2014, ApJ, 797, 138
Calzetti, D., Armus, L., Bohlin, R. C., et al. 2000, ApJ, 533, 682
Carniani, S., Maiolino, R., Pallottini, A., et al. 2017, A&A, 605, A42
Casey, C. M. 2012, MNRAS, 425, 3094
Charlot, S., & Fall, S. M. 2000, ApJ, 539, 718
Ciesla, L., Boselli, A., Elbaz, D., et al. 2016, A&A, 585, A43
Clements, D. L., Rigby, E., Maddox, S., et al. 2010, A&A, 518, L8
Cormier, D., Madden, S. C., Lebouteiller, V., et al. 2015, A&A, 578, A53
da Cunha, E., Charlot, S., & Elbaz, D. 2008, MNRAS, 388, 1595
da Cunha, E., Walter, F., Smail, I. R., et al. 2015, ApJ, 806, 110
Dale, D. A., Helou, G., Magdis, G. E., et al. 2014, ApJ, 784, 83
Díaz-Santos, T., Armus, L., Charmandaris, V., et al. 2017, ApJ, 846, 32
Downes, D, Solomon, P. M., & Radford, S. J. E. 1993, ApJL, 414, L13
Draine, B. T. 2003, ARA&A, 41, 241
Draine, B. T. 2011, Physics of the Interstellar and Intergalactic Medium
   (Princeton, NJ: Princeton Univ. Press)
Draine, B. T., & Li, A. 2007, ApJ, 657, 810
Ekström, S., Georgy, C., Eggenberger, P., et al. 2012, A&A, 537, A146
Farrah, D., Lebouteiller, V., Spoon, H. W. W., et al. 2013, ApJ, 776, 38
Ferkinhoff, C., Brisbin, D., Nikola, T., et al. 2011, ApJL, 740, L29
Ferkinhoff, C., Brisbin, D., Nikola, T., et al. 2015, ApJ, 806, 260
Ferkinhoff, C., Brisbin, D., Parshley, S., et al. 2014, ApJ, 780, 142
Ferkinhoff, C., Hailey-Dunsheath, S., Nikola, T., et al. 2010, ApJL, 714, L147
Ferkinhoff, C., Nikola, T., Parshley, S. C., et al. 2012, Proc. SPIE, 8452,
   845207
```

```
Fritz, J., Franceschini, A., & Hatziminaoglou, E. 2006, MNRAS, 366, 767
Genzel, R., Tacconi, L. J., Lutz, D., et al. 2015, ApJ, 800, 20
Graciá-Carpio, J., Sturm, E., Hailey-Dunsheath, S., et al. 2011, ApJL, 728, L7
Griffin, M. J., Abergel, A., Abreu, A., et al. 2010, A&A, 518, L3
Gullberg, B., De Breuck, C., Vieira, J. D., et al. 2015, MNRAS, 449, 2883
Güsten, R., Nyman, L. A., Schilke, P., et al. 2006, A&A, 454, 13
Hailey-Dunsheath, S. 2009, PhD thesis, Cornell Univ.
Hailey-Dunsheath, S., Nikola, T., Stacey, G. J., et al. 2010, ApJL, 714, L162
Harris, A. I., Baker, A. J., Frayer, D. T., et al. 2012, ApJ, 752, 152
Hodge, J. A., Swinbank, A. M., Simpson, J. M., et al. 2016, ApJ, 833, 103
Inoue, A. K., Tamura, Y., Matsuo, H., et al. 2016, Sci, 352, 1559
Kurucz, R. L. 1979, ApJS, 40, 1
Kurucz, R. L. 1993, yCat, 6039
Laporte, N., Ellis, R. S., Boone, F., et al. 2017, ApJL, 837, L21
Leitherer, C., Schaerer, D., Goldader, J. D., et al. 1999, ApJS, 123, 3
Leroy, A. K., Bolatto, A., Gordon, K., et al. 2011, ApJ, 737, 12
Madau, P., & Dickinson, M. 2014, ARA&A, 52, 415
Maraston, C. 2005, MNRAS, 362, 799
Marrone, D. P., Spilker, J. S., Hayward, C. C., et al. 2017, Natur, 553, 51
Martins, F., Schaerer, D., & Hillier, D. J. 2005, A&A, 436, 1049
Marton, G., Calzoletti, L., Perez Garcia, A. M., et al. 2017, arXiv:1705.05693
Neri, R., Genzel, R., Ivison, R. J., et al. 2003, ApJL, 597, L113
Noll, S., Burgarella, D., Giovannoli, E., et al. 2009, A&A, 507, 1793
Ott, S. 2010, in ASP Conf. Ser. 434, Astronomical Data Analysis Software and
  Systems XIX, ed. Y. Mizumoto, K.-I. Morita, & M. Ohishi (San Francisco,
  CA: ASP), 139
Parshley, S. C., Ferkinhoff, C., Nikola, T., et al. 2012, Proc. SPIE, 8452,
  84521R
Poglitsch, A., Waelkens, C., Geis, N., et al. 2010, A&A, 518, L2
Rigopoulou, D., Pereira-Santaella, M., Magdis, G. E., et al. 2018, MNRAS,
Rubin, R. H. 1985, ApJS, 57, 349
Rubin, R. H. 1989, ApJS, 69, 897
Schulz, B., Marton, G., Valtchanov, I., et al. 2017, arXiv:1706.00448
Scoville, N., Sheth, K., Aussel, H., et al. 2016, ApJ, 820, 83
Serra, P., Amblard, A., Temi, P., et al. 2011, ApJ, 740, 22
Solomon, P. M., & Vanden Bout, P. A. 2005, ARA&A, 43, 677
Speagle, J. S., Steinhardt, C. L., Capak, P. L., & Silverman, J. D. 2014, ApJS,
Spilker, J. S., Marrone, D. P., Aravena, M., et al. 2016, ApJ, 826, 112
Stacey, G. J., Hailey-Dunsheath, S., Ferkinhoff, C., et al. 2010, ApJ, 724, 957
Tacconi, L. J., Genzel, R., Saintonge, A., et al. 2018, ApJ, 853, 179
Tacconi, L. J., Neri, R., Genzel, R., et al. 2013, ApJ, 768, 74
Uzgil, B. D., Bradford, C. M., Hailey-Dunsheath, S., et al. 2016, ApJ, 832,
  209
Valtchanov, I., Virdee, J., Ivison, R. J., et al. 2011, MNRAS, 415, 3473
Wardlow, J. L., Cooray, A., Osage, W., et al. 2017, ApJ, 837, 12
Wright, E. L., Eisenhardt, P. R. M., Mainzer, A. K., et al. 2010, AJ, 140,
   1868
Yang, C., Omont, A., Beelen, A., et al. 2016, A&A, 595, A80
```